La Granja: Revista de Ciencias de la Vida
pISSN:1390-3799; eISSN:1390-8596
https://doi.org/10.17163/lgr.n41.2025.04

Scientific paper/ Artículo científico

Earth Sciences

Rainfall Characteristics and extreme events in the Tropical Andes using a Vertically Pointing rain radar

Características de lluvia y eventos extremos en los Andes Tropicales usando un radar de lluvia de Apuntamiento Vertical

Javier Chininín-Cabrera[1] and Rolando Célleri*[1,2]

[1]*Departamento de Recursos Hídricos y Ciencias Ambientales, Universidad de Cuenca, 010207, Cuenca, Ecuador.*
[2]*Facultad de Ingeniería, Universidad de Cuenca, 010203, Cuenca, Ecuador.*

*Corresponding author: rolando.celleri@ucuenca.edu.ec

Received on February 26th, 2023. Accepted, after revision on June 25th, 2024. Published on March 1st, 2025.

Abstract

Although the vertical structure of rain is relevant in aspects such as climate models (CM) and quantitative precipitation estimation (QPE), data about it is limited in the Andes. Within these aspects, extreme rainfall events are important due to their potential social impacts. Therefore, this study aims to characterize the vertical structure of rain and extreme events in the Tropical Andes using a Vertically Pointing Micro Rain Radar. For this, (i) the diurnal rainfall cycle was determined; (ii) the bright band was characterized; (iii) common characteristics of the vertical rain profile during extreme events, along with the average vertical reflectivity profiles of different development stages of a characteristic extreme event were studied. The study was performed using five years of data from a vertically pointing rain radar installed in Cuenca, Ecuador. The main results indicate that (i) rain events with high intensities are concentrated between 12:30 – 20:00 h (Local Time), during which 77% of the total rainfall occurs; (ii) the bright band has a thickness between 200 and 400 m, and its top (melting layer) is located between 4500 and 4900 m above sea level; (iii) rainfall shows a high variability in the water column: during the convective stage reflectivity values can increase up to 94% from the fusion layer to the ground. The results show the complexity of rainfall events in the Andean region and the need to consider these aspects into CM and QPE to improve their accuracy.

Keywords: Extreme events, melting layer, diurnal rainfall cycle, vertical structure of rain, tropical Andes.

Resumen

La información de la estructura vertical de la lluvia en los Andes es bastante limitada, a pesar de su importancia en aspectos como modelos de clima (MC) y estimación cuantitativa de lluvia (ECL). Dentro de estos aspectos, los eventos extremos conforman un punto de alto interés debido a la necesidad de mitigar los problemas sociales que pueden ocasionar. Por lo tanto, el objetivo de esta investigación es caracterizar la estructura vertical de la lluvia y eventos extremos en los Andes Tropicales usando un micro radar de lluvia de apuntamiento vertical. Para esto, (i) se determinó el ciclo diario de lluvia; (ii) se caracterizó la bright band; (iii) se caracterizó la columna de agua y los perfiles verticales promedio de reflectividad. Se utilizaron 5 años de datos medidos con un radar de apuntamiento vertical instalado en Cuenca, Ecuador. Los principales resultados indican que (i) los eventos de lluvia con altas intensidades se concentran entre las 12:30 – 20:00 h (Tiempo Local), y en este intervalo se registra el 77% del total de lluvia; (ii) la bright band tiene un espesor entre 200 y 400 m y su parte superior (capa de fusión) se ubica entre 4500 y 4900 m snm; y (iii) la lluvia muestra una alta variabilidad en la columna de agua: durante la etapa convectiva los valores de reflectividad pueden aumentar hasta en un 94% desde la capa de fusión hasta la superficie. Los resultados evidencian la alta complejidad de los eventos de lluvia de la zona andina y la necesidad de considerar estos aspectos para mejorar la precisión de MC y ECL.

Palabras clave: Eventos extremos, capa de fusión, ciclo diario de lluvia, estructura vertical de lluvia, Andes tropicales.

Suggested citation: Chininín-Cabrera, J. and Célleri, R. (2025). Rainfall Characteristics and extreme events in the Tropical Andes using a Vertically Pointing rain radar. *La Granja: Revista de Ciencias de la Vida.* Vol. 41(1):69-81. https://doi.org/10.17163/lgr.n41.2025.04.

Orcid IDs:

Javier Chininín-Cabrera: https://orcid.org/0000-0003-3412-5576
Rolando Célleri: https://orcid.org/0000-0002-7683-3768

1 Introduction

Extreme rainfall events pose a significant challenge to society due to their potential consequences, such as flash floods, crop damage, erosion, landslides, and water contamination (Barlow et al., 2019; Mukherjee et al., 2018). This makes it essential to understand, characterize, and accurately estimate these events to mitigate their effects. However, in the Andes, the detailed study of such events and the processes governing rainfall has been limited by the sparse and unevenly distributed monitoring systems (Perry et al., 2017; Seidel et al., 2019) and by the fact that rainfall properties vary on temporal scales shorter than those captured by available climate data and models (Boucher et al., 2013; Seidel et al., 2019; Ward et al., 2011).

This issue increases by the high spatiotemporal variability of rainfall processes, influenced by the region's complex topography (Orellana-Alvear et al., 2017; Yarleque et al., 2016). These challenges are especially observed in the limited data and studies available on the Andes' vertical structure of rainfall (VSR), which describes rainfall from its origin in the clouds to when it reaches the ground.

The study of VSR has a significant impact on various aspects. First, it helps to understand the microphysics governing rainfall formation and evolution (Durán-Alarcón et al., 2019; Urgilés et al., 2021); moreover, features such as the bright band (BB) allow estimating the altitude at which rainfall originates, as it serves as an indicator of the melting layer (Endries et al., 2018; Konwar et al., 2012; Sumesh et al., 2019). In mountainous regions, radar and satellite products often suffer from accuracy deficiencies (Chen et al., 2022; Orellana-Alvear et al., 2019; Satgé et al., 2019; Ward et al., 2011), primarily due to the difference in altitude between the measurement location and the ground.

These inaccuracies are typically corrected using ground-based rain gauge data, but often without considering the vertical variation of rainfall properties (e.g., reflectivity) in the atmospheric column (Das and Maitra, 2016; Kirstetter et al., 2013; Peters et al., 2005). Therefore, the VSR provides crucial information for improving, comparing, and validating climate models and estimates obtained from radars and satellites (Durán-Alarcón et al., 2019).

Ground-based vertically pointing radars offer a suitable alternative for obtaining VSR data (Durán-Alarcón et al., 2019; Luo et al., 2020; Urgilés et al., 2021). In the Tropical Andes, studies using these radars are limited and can be classified into two groups: those directly describing the VSR and those using VSR for other purposes. In the first group, research has primarily focused on the melting layer or BB. Perry et al. (2017) calculated the frequency distribution of the melting layer height for Cusco, Peru (August 2014 – February 2015) and La Paz, Bolivia (October 2015 – December 2015), finding that most measurements in both locations fall between 4400 and 5100 meters above sea level (masl). Endries et al. (2018) used the same dataset for Cusco and an extended one for La Paz (October 2015 – February 2017) to study BB height based on time of day, finding that, consistent with surface temperature, it is higher in the afternoon and early evening. They also observed that the El Niño phenomenon in La Paz may have contributed to an increase in BB height during the 2015–2016 period.

Finally, Kumar et al. (2020) in Huancayo, Peru (2015–2018), reported that the BB is mostly found between 4000 and 5000 masl, but also, for the first time, determined the vertical variation of rainfall properties (reflectivity, intensity, liquid water content, and drop size distribution) for different surface rainfall intensities, revealing interesting behaviors especially for high intensities (20–200 mm/h). The second group of studies has focused mainly on classifying rainfall as stratiform, convective, or mixed using VSR, as done by Seidel et al. (2019) and Urgilés et al. (2021). Additionally, Bendix et al. (2006) in Loja, Ecuador, showed that mixed rainfall is a key feature of the region's precipitation, while Schauwecker et al. (2017), using the same dataset as Perry et al. (2017), determined that when the surface temperature is below 15°C, the melting layer can be relatively estimated using extrapolations with reanalysis data.

As noted, VSR information in the Tropical Andes obtained directly from ground-based radars is quite limited and is primarily concentrated in Peru and Bolivia. Furthermore, in no cases has VSR been used to study rainfall generation and dynamics during extreme events, despite its importance for both societal concerns and rainfall models and estimates.

Therefore, the objective of this research is to characterize the vertical structure of rainfall and extreme events in the Tropical Andes using a vertically pointing micro rain radar located in Cuenca, Ecuador. To achieve this, the study aims to (i) characterize the distribution of rainfall events throughout the day, especially those of high intensity, based on the study of the diurnal rainfall cycle; (ii) characterize the bright band based on its key features; and (iii) characterize the atmospheric column during extreme rainfall events and their temporal evolution.

2 Methodology

2.1 Study Area and Equipment

The study was conducted using data collected at the Balzay Meteorological Observatory (2°53′32″ S, 79°02′10″ W), located at 2600 meters above sea level in the Andes of Ecuador, in the city of Cuenca (Figure 1). The region experiences a bimodal precipitation pattern, with rainy months occurring in March-April and October-November (Campozano et al., 2016).

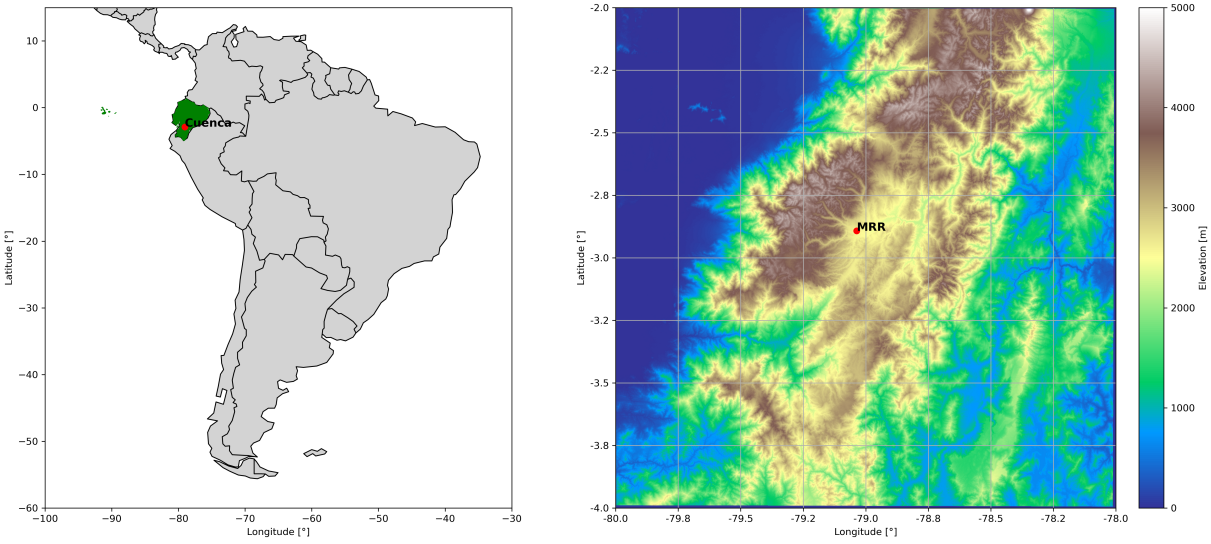

Figure 1. Study area in the Ecuadorian Andes.

The data used in this study come from a Micro Rain Radar (MRR), a compact radar with a vertically pointing parabolic antenna, operating at a frequency of 24 GHz, a wavelength of 12.5 mm, and an FM-CW operating mode (Löffler-Mang et al., 1999; METEK, 2009; Peters et al., 2002). The MRR uses the Doppler velocity spectrum as its measurement principle and derives the drop size distribution through the analytical relationship between terminal velocity and drop diameter, as described by Atlas et al. (1973). Based on this variable, the MRR calculates rainfall parameters such as reflectivity, liquid water content, rain intensity, and drop fall velocity; these relationships can be reviewed in detail in METEK (2009) and Peters et al. (2005). In each radar measurement, the atmospheric column is vertically discretized into 31 equal parts (bins), and for each bin, the five aforementioned variables are obtained. This measurement is referred to as the vertical profile (VP).

2.2 Data and Preprocessing

Five years of MRR measurements, from February 2017 to January 2022, were used. The MRR observations had a temporal resolution of 1 minute and an altitudinal resolution (bin thickness) of 100 meters. The MRR measures precipitation up to an altitude of 3100 meters above ground level (i.e., from 2600 to 5700 meters above sea level). The variables used in this study were reflectivity and rain intensity. To fill gaps and eliminate outliers in the rain intensity measurements at the lowest bin, data from a laser disdrometer (Thies Clima Laser) located at the same

meteorological observatory were used. The percentage of missing measurements for this variable was reduced from 15.7% to 6.0%. A linear correlation was performed between the 5-minute accumulated rainfall from both instruments (Figure 2). Although the MRR measures the average intensity in a 100-meter bin from the surface, its variability can be explained by the disdrometer by 80%, as indicated by the coefficient of determination (R^2); furthermore, the p-value is less than 0.001.

On the other hand, no gap filling was applied to the vertical profiles (VP); however, a quality control process was implemented to remove incomplete measurements (i.e., VPs with one or more missing bins). Additionally, the two highest bins of the VPs were excluded from all analyses, as they often presented outliers due to electromagnetic interference.

2.3 Calculation of the Diurnal Rainfall Cycle

The characteristics of the diurnal rainfall cycle were studied in 30-minute intervals using the average precipitation amount (PA), precipitation frequency (PF), average precipitation intensity (PI), and accumulated average precipitation (PAQ). Based on the considerations of Zhou et al. (2008) and Zhang et al. (2017), PA was calculated for each 30-minute interval during the 5-year study period by dividing the accumulated precipitation by the number of valid measurements. PF was calculated as the ratio between the number of rainy measurements and the number of valid measurements, while PI was obtained by dividing the accumulated precipitation by the number of rainy measurements. Additionally, PAQ was calculated as the accumulated percentage of the total rainfall up to each interval. For this study, a 30-minute measurement was considered valid if 90% or more of the minutes within that interval had data, and considered rainy if a minimum of 0.1 mm of precipitation was recorded.

2.4 Characterization of the Bright Band

The bright band (BB) was characterized by analyzing its thickness (BB_{th}) and the height of its upper boundary (melting layer; H_T), and how these two characteristics varied during the study period was calculated. To detect the presence of the BB during an event, the algorithm proposed by Cha et al. (2009) was implemented, which builds on previous studies by Klaassen (1988) and Fabry and Zawadzki (1995) but introduces a new concept called bright band sharpness. This algorithm is based on the use of the reflectivity VP and the variation in its gradient.

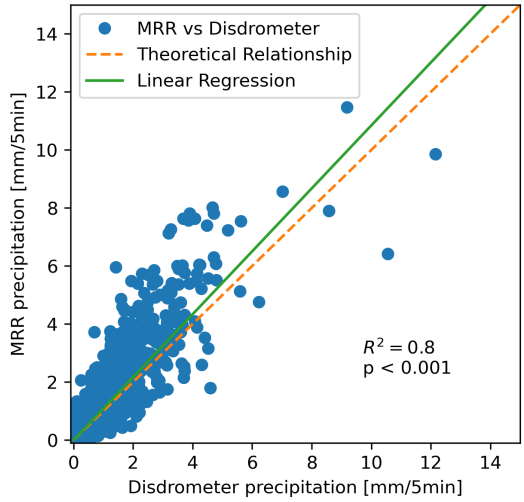

Figure 2. Correlation of cumulative rainfall every 5 minutes between disdrometer and MRR measurements in its first band above ground level (0-100 masl).

When the BB is detected in a measurement, H_T is defined as the altitude with the steepest negative gradient, and similarly, the lower boundary (H_B) is the altitude with the steepest positive gradient; BB_{th} is calculated as the difference between H_T and H_B. Additionally, the algorithm requires the peak reflectivity (Z_{peak}) from the VP; to obtain this, the first 500 meters from the ground were excluded, as it was verified that in some cases, Z_{peak} occurred at these heights (this is mainly due to coalescence and aggregation processes at these levels during different events, which can significantly increase reflectivity, exceeding that of the BB), which would erroneously discard a VP with an actual BB.

2.5 Vertical Rainfall Variability

The evolution of the reflectivity VP was visually inspected for all events where rain intensities greater than 100 mm/h per minute were recorded in the first bin. This threshold captures approximately the top 10.0 % of the highest-intensity events recorded per minute during the study period, categorizing them as extreme rainfall events. From these, one representative high-intensity rainfall event was selected, and the characteristics of its average vertical reflectivity profile (AVRP) were thoroughly studied during its various developmental stages.

For each stage, the AVRP was calculated as the average reflectivity of each bin in the VPs, as shown by Das and Maitra (2016) and Peters et al. (2005). The developmental stages were classified as convective, stratiform with BB, and stratiform without BB. To distinguish between convective and stratiform stages, vertical velocity profiles and a fuzzy rule-based system were used, as described in Seidel et al. (2019). Measurements that could not be classified using this methodology were labeled as "Unclassified." Additionally, for the sub-classification of the stratiform stage, BB detection was performed using the algorithm described in Section 2.4.

3 Results

3.1 Diurnal rainfall cycle

Figure 3 shows the curves for precipitation amount (PA), precipitation frequency (PF), precipitation intensity (PI), and accumulated precipitation amount (PAQ) for the diurnal rainfall cycle. PA and PI clearly demonstrate the region's rainfall pattern, which exhibits a unimodal behavior, with the highest peaks occurring around 15:00 local time (LT; UTC-5). PA indicates that the accumulated rainfall for each interval begins to increase significantly after 12:30 LT and stabilizes around 20:00 LT, remaining relatively low during the rest of the day. Furthermore, 77 % of the total rainfall occurs within this 7.5-hour window, as indicated by PAQ. Similarly, PI shows that the maximum average intensities, around 4 mm/h, are recorded between 14:00 and 14:30 LT.

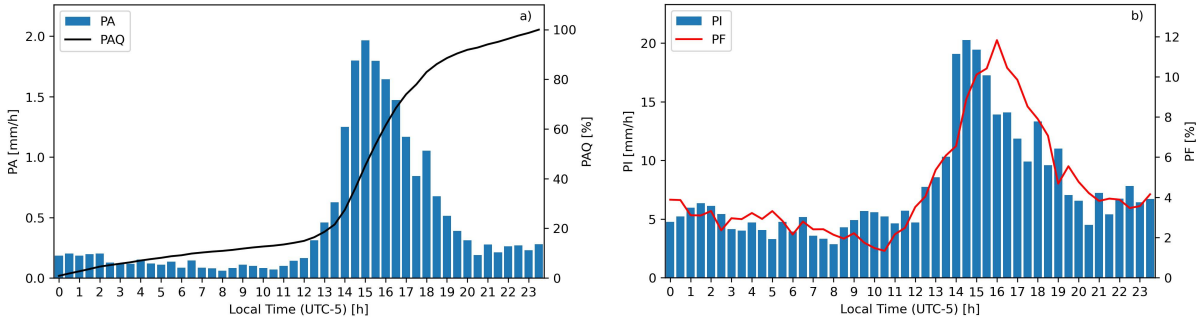

Figure 3. Diurnal rainfall cycle for the period 02/01/2017 – 01/31/2022. a) Precipitation amount (PA) and accumulated precipitation amount (PAQ); b) Precipitation frequency (PF) and precipitation intensity (PI).

While this intensity might be considered low, it should be noted that it represents the average of all events measured during this interval. The magnitude of the events occurring as well as in adjacent intervals can be seen by comparing PF and PA, as PF is approximately three times higher than during the night or morning hours, yet the accumulated rainfall can be up to 20 times greater. This suggests that high-intensity events occurring during these hours contribute significantly to the total precipitation.

3.2 Characterization of the Bright Band

Figure 4 presents the characterization of the BB in terms of a) Diurnal cycle, b) Variation and frequency of its upper boundary height (H_T) and c) Variation and frequency of its thickness (BB_{th}). The lowest occurrence of the BB is found between 09:00 and 12:00 LT. After this period, its frequency increases, reaching a peak at 18:00 LT, after which it begins to decline until the cycle repeats (Figure 4a).

On the other hand, H_T and BB_{th} exhibit relatively stable behavior, with variations centered around typical values. In the case of H_T (Figure 4b), it is found between 4500 and 4900 meters above sea level in 94.5%. Meanwhile, BB_{th} (Figure 4c) ranges between 200 and 400 meters 93.4% of the time. These characteristics indicate the height of the melting layer (where rain originates) and the distance required to complete the melting process of ice or snow into rain in the region. Additionally, the range of variation for H_T aligns with previous studies in the Andes of Bolivia and Peru (Endries et al., 2018; Kumar et al., 2020; Perry et al., 2017), indicating the stability of this height. The greatest differences are observed in southern Peru, where higher altitudes are recorded during the austral summer, which according to Schauwecker et al. (2017), may be caused by the Bolivian high-pressure system.

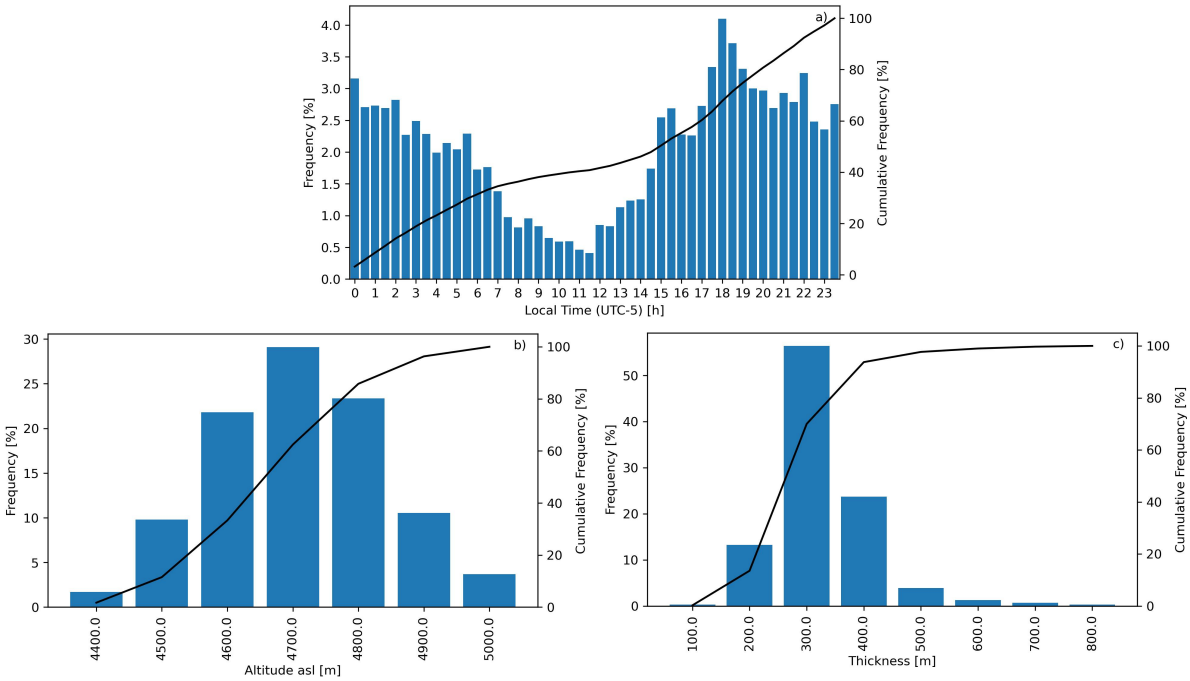

Figure 4. Characteristics of the bright band during the period 02/01/2017 – 01/31/2022. a) Diurnal cycle; b) Variation and frequency of its upper boundary height (H_T); c) Variation and frequency of its thickness (BB_{th}).

3.3 Vertical Rainfall Variability in Extreme Events

During the entire study period, there were 30 high-intensity rainfall events in which surface intensities exceeded 100 mm/h in a minute. All of these events exhibited convective stages during their evolution, with 90% doing so in the early minutes of the storm, rapidly reaching high reflectivities of around 40 dBZ. Additionally, 50% of the events displayed exclusively convective behavior, while the rest showed a combination of convective and stratiform stages. Out of the latter group, 80% exhibited stratiform stages with a BB, which typically developed at the end of the storm.

On December 28, 2017, an event occurred that contained many of the characteristics mentioned above, and it was selected as a case study. Figure 5 shows the time evolution of its reflectivity profile, and the color bar above indicates the moments when convective stages, stratiform stages with BB, and stratiform stages without BB were recorded. Seidel et al. (2019) used this same event to illustrate the results of the methodology, described in section 2.5, for classifying storms into their convective or stratiform stages. Therefore, the analysis performed in this study also complements that work.

The average vertical reflectivity profiles (AVRP) for the different stages of the case study are shown in Figure 6. The AVRP for the convective stage presents significant differences compared to the stratiform stages, as it shows a much steeper negative gradient below 4700 meters above sea level. This results in a considerable increase in reflectivity from the melting layer to the surface (93.7%), primarily due to the vertical winds characteristic of convective events, which promote rapid droplet growth with coalescence and aggregation processes dominating over others (Luo et al., 2020; Ramadhan et al., 2020; Rosenfeld and Ulbrich, 2003; Wen et al., 2017).

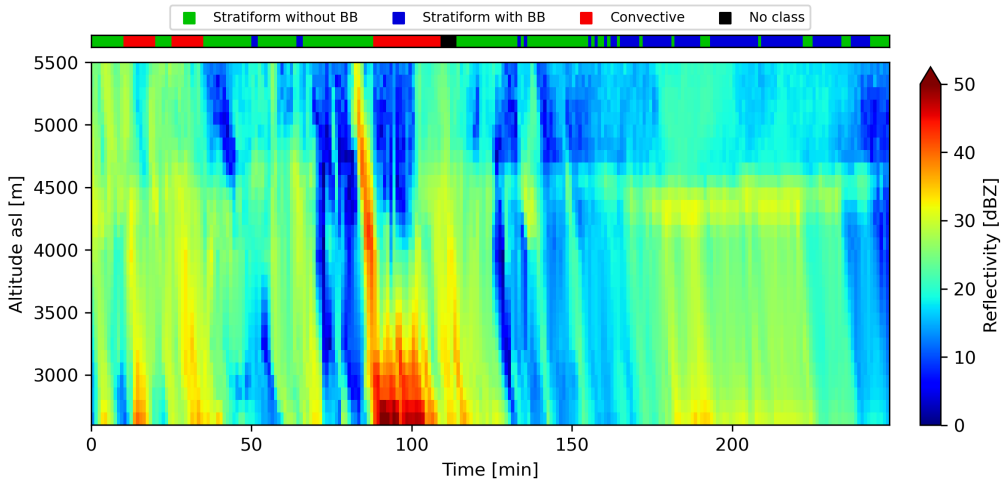

Figure 5. Vertical Reflectivity Profile and Development Stages of the Event Recorded on December 28, 2017, Between 14:50 and 19:10 LT.

In the case of the stratiform stages, the AVRP shows a significant increase in reflectivity between 4700 and 4200 meters above sea level, indicating that the rain is generated by the melting process (Massmann et al., 2017). However, the behavior diverges after reaching maximum reflectivity within this range, suggesting that rapid droplet growth occurs during the stage without BB, maintaining reflectivity close to its maximum. Additionally, the AVRP for these stages behaves similarly below 4200 meters above sea level, with relatively constant values until approaching the surface, where a negative gradient appears. This stable behavior is due to the balance between coalescence, droplet breakup, and evaporation processes, while the increase in reflectivity near the surface is explained by the dominance

of coalescence and aggregation processes (Luo et al., 2020; Ramadhan et al., 2020; Wen et al., 2017). Above 4700 meters above sea level, all AVRPs exhibit relatively similar and constant behavior. This is likely because water exists in a solid state at this altitude, as described in Section 3.2, where the melting layer is generally located.

4 Discussion

4.1 Variability of Rainfall Characteristics

The diurnal rainfall cycle is consistent with previous results reported by Yang and Smith (2006), which found that peak rainfall tends to occur in the mid-afternoon in the continental tropics. The unimodal pattern of the diurnal cycle highlights the significant influence of afternoon convective events, mainly driven by surface heating (Bendix et al., 2006; Perry et al., 2014). In fact, all 30 extreme events identified during the study period occurred between 12:30 and 20:00 LT. This finding aligns with Hernandez-Deckers (2022), who showed that in northwestern South America (including parts of Ecuador), the diurnal cycle of convective events closely follows the pattern of PA.

It is worth noting that bimodal behaviors, with peaks in the early morning and late afternoon/evening, have been reported in the eastern foothills of the Andes in Colombia, Peru, and southern Ecuador. These behaviors are generally due to mesoscale instabilities (Bendix et al., 2006; Endries et al., 2018; Kumar et al., 2020, 2019; Poveda et al., 2005; Seidel et al., 2019).

On the other hand, low-intensity events, such as stratiform rainfall with or without BB, also play a significant role in the diurnal cycle. As Seidel et al. (2019) revealed, 91.9% of rainfall measurements in the region are stratiform, and 37.2% of those have BB. Their diurnal cycle (Figure 4a) shows persistent occurrence throughout the day, except in the mornings. This high frequency and persistence are particularly evident outside the 12:30–20:00 LT window, where rainfall amount and frequencies remain relatively low and stable.

4.2 Vertical Reflectivity Variability and Its Influence on Rainfall Estimates

While the vertical reflectivity variability reported in detail via AVRP in this study is limited to the case study, it highlights the importance of considering all event evolution stages for such analyses. Previous studies, such as Das and Maitra (2016), Kumar et al. (2020) and Peters et al. (2005), analyzed AVRP by grouping VPs according to surface rainfall intensity. However, this approach might lead to information loss in stratiform events with BB. This is because profiles with and without BB are averaged, potentially masking the reflectivity peak (Figure 6), which could lead to surface overestimations, as discussed later.

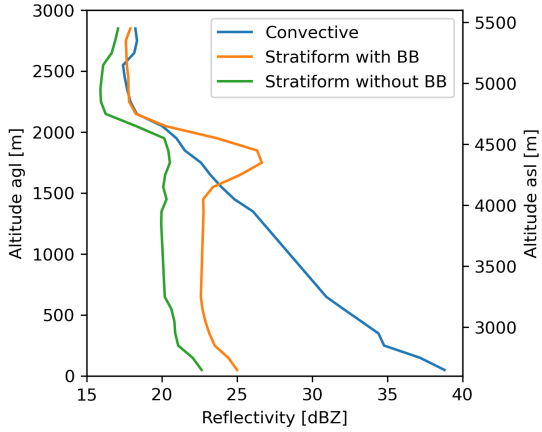

Figure 6. Average vertical reflectivity profiles (AVRP) for the stages of the storm recorded on December 28, 2017, between 14:50 and 19:10 LT

Conversely, grouping VPs according to event evolution stages, as done in this study, could also omit information for low-intensity events, where evaporation is more likely, leading to a positive gradient in the reflectivity VP, as shown in Das and Maitra (2016) and Kumar et al. (2020) for intensities between 0.02 and 2 mm/h. This type of gradient was not observed in this study's results, possibly due to specific event conditions or the averaging of VPs with opposite gradients.

In this context, we have found that reflectivity varies greatly within the atmospheric column and throughout the different stages of rainfall events. This underscores the need to account for these variations when estimating rainfall using ground-based radars or satellites in the region, as potential errors may arise depending on the altitude at which measurements are taken. Rainfall underestimation could occur due to: 1) Measurements above the melting layer during any stage of the event, as shown in the case study, where reflectivity above 4700 meters was lower than at the surface, with the greatest difference being 122.8%; and 2) Steep negative gradients in convective stages, where below the melting layer, this gradient caused a 93.7% increase in reflectivity down to the surface in the case study. On the other hand, overestimation can occur during stratiform stages at the BB height due to the reflectivity peak at that level, which does not represent surface conditions. Additionally, if evaporation occurs near the surface, this overestimation could be exacerbated because surface reflectivity would decrease, and the difference with the BB would be much greater than in the case study (Figure 6).

To avoid such errors, it would be ideal to classify the event as convective or stratiform—with or without BB—before estimating rainfall using Z–R relationships calibrated for these types, incorporating their vertical evolution and corresponding zone. However, this could be limited by the need for a network of instruments capable of making these classifications at multiple points. This highlights the importance of using new methods for estimating rainfall based on ground-based radar measurements, such as that shown in Orellana-Alvear et al. (2019), which improves the accuracy of the CAXX radar using estimates from random forest, a supervised machine learning algorithm. These models may indirectly account for differences based on rainfall types.

Based on the above, future research is recommended to compare the approaches for grouping VPs, either by intensity or by rainfall type. This will help determine the best way to group them to characterize their vertical evolution with the least amount of information loss. This will also be important for improving rainfall estimates using both traditional and alternative methods, as more efficient VP groupings could yield calibrated Z–R relationships, and if feasible, artificial intelligence models for each group.

5 Conclusions

The objective of this research was to characterize the vertical structure of rainfall and extreme events at one of the few sites in the Andes equipped with ground-based vertically pointing radars. To achieve this, the diurnal rainfall cycle was determined, the bright band was characterized, common features in the atmospheric column during high-intensity events were studied, and the average vertical reflectivity profiles of a representative event were analyzed. Based on this, the following conclusions can be drawn:

High-intensity events occur in the afternoon and are responsible for shaping the unimodal diurnal rainfall cycle, with a peak at 15:00. Seventy-seven percent of the total rainfall is recorded between 12:00 and 20:00 LT.

The BB exhibits consistent behavior and characteristics throughout the study period: (i) in 94.5% of cases, its upper boundary (melting layer) is located between 4500 and 4900 meters above sea level; (ii) 93.4% of the time, it has a thickness of 200 to 400 meters; and (iii) its diurnal cycle shows a significant decrease in occurrence only in the mornings.

High-intensity rainfall events are primarily sudden, as 90% of the studied events experienced a sharp increase in reflectivity immediately after the storm began. Additionally, half of the intense events exhibited combined convective-stratiform behavior.

Reflectivity exhibits high variability in the atmospheric column during high-intensity rainfall

events. During the convective stage, reflectivity values can increase by up to 94% from the melting layer to the surface.

Acknowledgments

This study was part of the SDG^{nexus} Network project (grant number 57526248), funded by the German Academic Exchange Service (DAAD) with support from the Federal Ministry for Economic Cooperation and Development (BMZ) under the "exceed - Excellence in Development Cooperation" program. The University of Cuenca co-financed this research through the Vice-Rectorate for Research.

Author Contribution

J.C.C.: Data curation, formal analysis, investigation, software, writing – original draft; R.C.: Conceptualization, funding acquisition, methodology, supervision, validation, writing – review and editing.

References

Atlas, D., Srivastava, R., and Sekhon, R. (1973). Doppler radar characteristics of precipitation at vertical incidence. *Reviews of Geophysics*, 11(1):1–35. Online:https://n9.cl/8t5da7.

Barlow, M., Gutowski, W., Gyakum, J., Katz, R., Lim, Y., Schumacher, R., Wehner, M., Agel, L., Bosilovich, M., Collow, A., Gershunov, A., Grotjahn, R., Leung, R., Milrad, S., and Min, S. (2019). North american extreme precipitation events and related large-scale meteorological patterns: a review of statistical methods, dynamics, modeling, and trends. *Climate Dynamics*, 53:6835–6875. Online:https://n9.cl/jovyd.

Bendix, J., Rollenbeck, R., and Reudenbach, C. (2006). Diurnal patterns of rainfall in a tropical andean valley of southern ecuador as seen by a vertically pointing k-band doppler radar. *International Journal of Climatology: A Journal of the Royal Meteorological Society*, 26(6):829–846. Online:https://n9.cl/57h73.

Boucher, O., Randall, D., Artaxo, P., Bretherton, C., Feingold, G., Forster, P., Kerminen, V., Kondo, Y., Liao, H., and Lohmann, U. (2013). *Climate change 2013: The physical science basis. Contribution of working group I to the fifth assessment report of the intergovernmental panel on climate change*, chapter Clouds and aerosols, pages 571–657. Cambridge University Press.

Campozano, L., Célleri, R., Trachte, K., Bendix, J., and Samaniego, E. (2016). Rainfall and cloud dynamics in the andes: A southern ecuador case study. *Advances in Meteorology*, 2016(1):3192765. Online:https://n9.cl/6c7l1.

Cha, J. W., Chang, K. H., Yum, S., and Choi, Y. J. (2009). Comparison of the bright band characteristics measured by micro rain radar (mrr) at a mountain and a coastal site in south korea. *Advances in Atmospheric Sciences*, 26:211–221. Online:https://n9.cl/4214z.

Chen, M., Huang, Y., Li, Z., Larico, A., Xue, M., Hong, Y., Hu, X., Novoa, H., Martin, E., McPherson, R., Zhang, J., Gao, S., Wen, Y., Perez, A., and Morales, I. (2022). Cross-examining precipitation products by rain gauge, remote sensing, and wrf simulations over a south american region across the pacific coast and andes. *Atmosphere*, 13(10):1666. Online:https://n9.cl/xfegq.

Das, S. and Maitra, A. (2016). Vertical profile of rain: Ka band radar observations at tropical locations. *Journal of Hydrology*, 534:31–41. Online:https://n9.cl/ldgsx.

Durán-Alarcón, C., Boudevillain, B.and Genthon, C., Grazioli, J., Souverijns, N., van Lipzig, N., Gorodetskaya, I., and Berne, A. (2019). The vertical structure of precipitation at two stations in east antarctica derived from micro rain radars. *The Cryosphere*, 13(1):247–264. Online:https://n9.cl/5c4zcy.

Endries, J., Perry, L., Yuter, S., Seimon, A., Andrade-Flores, M., Winkelmann, R., Quispe, N., Rado, M., Montoya, N., and Velarde, F. (2018). Radar-observed characteristics of precipitation in the tropical high andes of southern peru and bolivia. *Journal of Applied Meteorology and Climatology*, 57(7):1441–1458. Online:https://n9.cl/69im8.

Fabry, F. and Zawadzki, I. (1995). Long-term radar observations of the melting layer of precipitation and their interpretation. *Journal of the atmospheric sciences*, 52(7):838–851. Online:https://n9.cl/la1qq.

Hernandez-Deckers, D. (2022). Features of atmospheric deep convection in northwestern south america obtained from infrared satellite data. *Quarterly Journal of the Royal Meteorological Society*, 148(742):338–350. Online:https://n9.cl/ehh79.

Kirstetter, P., Andrieu, H., Boudevillain, B., and Delrieu, G. (2013). A physically based identification of vertical profiles of reflectivity from volume scan radar data. *Journal of applied meteorology and climatology*, 52(7):1645–1663. Online:https://n9.cl/w6d92h.

Klaassen, W. (1988). Radar observations and simulation of the melting layer of precipitation. *Journal of Atmospheric Sciences*, 45(24):3741–3753. Online:https://n9.cl/p5x3q.

Konwar, M., Maheskumar, R., Das, S., and Morwal, S. (2012). Nature of light rain during presence and absence of bright band. *Journal of earth system science*, 121:947–961. Online:https://n9.cl/38t3f.

Kumar, S., Castillo-Velarde, C., Valdivia Prado, J., Flores Rojas, J., Callañaupa Gutierrez, S., Moya Alvarez, A., Martine-Castro, D., and Silva, Y. (2020). Rainfall characteristics in the mantaro basin over tropical andes from a vertically pointed profile rain radar and in-situ field campaign. *Atmosphere*, 11(3):248. Online:https://n9.cl/cqkjhd.

Kumar, S., Vidal, Y., Moya-Álvarez, A., and Martínez-Castro, D. (2019). Effect of the surface wind flow and topography on precipitating cloud systems over the andes and associated amazon basin: Gpm observations. *Atmospheric Research*, 225:193–208. Online:https://n9.cl/dpba8.

Löffler-Mang, M., Kunz, M., and Schmid, W. (1999). On the performance of a low-cost k-band doppler radar for quantitative rain measurements. *Journal of Atmospheric and Oceanic Technology*, 16(3):379–387. Online:https://n9.cl/gq699.

Luo, L., Xiao, H., Yang, H., Chen, H., Guo, J., Sun, Y., and Feng, L. (2020). Raindrop size distribution and microphysical characteristics of a great rainstorm in 2016 in beijing, china. *Atmospheric Research*, 239:104895. Online:https://n9.cl/991oo.

Massmann, A., Minder, J., Garreaud, R., Kingsmill, D., Valenzuela, R.and Montecinos, A., and Fults, S.and Snider, J. (2017). The chilean coastal orographic precipitation experiment: Observing the influence of microphysical rain regimes on coastal orographic precipitation. *Journal of Hydrometeorology*, 18(10):2723–2743. Online:https://n9.cl/6yykb4.

METEK (2009). *MRR Physical Basics, Valid for MRR Service Version 5.2.0.1*.

Mukherjee, S., Aadhar, S., Stone, D., and Mishra, V. (2018). Increase in extreme precipitation events under anthropogenic warming in india. *Weather and climate extremes*, 20:45–53. Online:https://n9.cl/ilr75.

Orellana-Alvear, J., Célleri, R., Rollenbeck, R., and Bendix, J. (2017). Analysis of rain types and their z–r relationships at different locations in the high andes of southern ecuador. *Journal of Applied Meteorology and Climatology*, 56(11):3065–3080. Online:https://n9.cl/aujfbd.

Orellana-Alvear, J., Célleri, R., Rollenbeck, R., and Bendix, J. (2019). Optimization of x-band radar rainfall retrieval in the southern andes of ecuador using a random forest model. *Remote Sensing*, 11(14):1632. Online:https://n9.cl/2jmom.

Perry, L., Seimon, A., Andrade-Flores, M., Endries, J., Yuter, S., Velarde, F., Arias, S., Bonshoms, M., Burton, E., Winkelmann, I., Cooper, C., Mamani, G., Rado, M., Montoya, N., and Quispe, N. (2017). Characteristics of precipitating storms in glacierized tropical andean cordilleras of peru and bolivia. *Annals of the American Association of Geographers*, 107(2):309–322. Online:https://n9.cl/tmmwu.

Perry, L., Seimon, A., and Kelly, G. (2014). Precipitation delivery in the tropical high andes of southern peru: new findings and paleoclimatic implications. *International journal of Climatology*, 34(1):197–215. Online:https://n9.cl/deq83.

Peters, G., Fischer, B., and Andersson, T. (2002). Rain observations with a vertically looking micro rain radar (mrr). *Boreal environment research*, 7(4):353–362. Online:https://n9.cl/g4ihk.

Peters, G., Fischer, B., Münster, H., Clemens, M., and Wagner, A. (2005). Profiles of raindrop size distributions as retrieved by microrain radars. *Journal of Applied Meteorology and Climatology*, 44(12):1930–1949. Online:https://n9.cl/6lmqb.

Poveda, G., Mesa, O., Salazar, L., Arias, P., Moreno, H., Vieira, S., Agudelo, P., Toro, V., and Alvarez, J. (2005). The diurnal cycle of precipitation in the tropical andes of colombia. *Monthly Weather Review*, 133(1):228–240. Online:https://n9.cl/1rc7k.

Ramadhan, R., Marzuki, V., Vonnisa, M., Harmadi, Hashiguchi, H., and Shimomai, T. (2020). Diurnal variation in the vertical profile of the raindrop size distribution for stratiform rain as inferred from micro rain radar observations in sumatra. *Advances in Atmospheric Sciences*, 37:832–846. Online:https://n9.cl/tyyg4m.

Rosenfeld, D. and Ulbrich, C. (2003). *Radar and Atmospheric Science: A Collection of Essays in Honor of David Atlas*, chapter Cloud microphysical properties, processes, and rainfall estimation opportunities, page 237–258. Cambridge University Press.

Satgé, F., Ruelland, D., Bonnet, M., Molina, J., and Pillco, R. (2019). Consistency of satellite-based precipitation products in space and over time compared with gauge observations and snow-hydrological modelling in the lake titicaca region. *Hydrology and Earth System Sciences*, 23(1):595–619. Online:https://n9.cl/0iimn.

Schauwecker, S., Rohrer, M., Huggel, C., Endries, J., Montoya, N., Neukom, R., Perry, B., Salzmann, N., Schwarb, M., and Suarez, W. (2017). The freezing level in the tropical andes, peru: An indicator for present and future glacier extents. *Journal of Geophysical Research: Atmospheres*, 122(10):5172–5189. Online:https://n9.cl/nge5k.

Seidel, J., Trachte, K., Orellana-Alvear, J., Figueroa, R., Célleri, R., Bendix, J., Fernandez, C., and Huggel, C. (2019). Precipitation characteristics at two locations in the tropical andes by means of vertically pointing micro-rain radar observations. *Remote Sensing*, 11(24):2985. Online:https://n9.cl/rbmsh.

Sumesh, R., Resmi, E., Unnikrishnan, C., Jash, D., Sreekanth, T., Resmi, M., Rajeevan, K., Nita, S., and Ramachandran, K. (2019). Microphysical aspects of tropical rainfall during bright band events at mid and high-altitude regions over southern western ghats, india. *Atmospheric Research*, 227:178–19. Online:https://n9.cl/xjsco.

Urgilés, G., Célleri, R., Trachte, K., Bendix, J., and Orellana-Alvear, J. (2021). Clustering of rainfall types using micro rain radar and laser disdrometer observations in the tropical andes. *Remote Sensing*, 13(5):991. Online:https://n9.cl/wf0eoo.

Ward, E., Buytaert, W., Peaver, L., and Wheater, H. (2011). Evaluation of precipitation products over complex mountainous terrain: A water resources perspective. *Advances in water resources*, 34(10):1222–1231. Online:https://n9.cl/yb56c.

Wen, G., Xiao, H., Yang, H., Bi, Y., and Xu, W. (2017). Characteristics of summer and winter precipitation over northern china. *Atmospheric Research*, 197:390–406. Online:https://n9.cl/6mesf.

Yang, S. and Smith, E. (2006). Mechanisms for diurnal variability of global tropical rainfall observed from trmm. *Journal of climate*, 19(20):5190–5226. Online:https://n9.cl/r7p5o.

Yarleque, C., Vuille, M., Hardy, D., Posadas, A., and Quiroz, R. (2016). Multiscale assessment of spatial precipitation variability over complex mountain terrain using a high-resolution spatiotemporal wavelet reconstruction method. *Journal of Geophysical Research: Atmospheres*, 121(20):12–198. Online:https://n9.cl/atmk4.

Zhang, W., Huang, A., Zhou, Y., Yang, B., Fang, D., Zhang, L., and Wu, Y. (2017). Diurnal cycle of precipitation over fujian province during the presummer rainy season in southern china. *Theoretical and Applied Climatology*, 130:993–1006. Online:https://n9.cl/0tzid4.

Zhou, T., Yu, R., Chen, H., Dai, A., and Pan, Y. (2008). Summer precipitation frequency, intensity, and diurnal cycle over china: A comparison of satellite data with rain gauge observations. *Journal of Climate*, 21(16):3997–4010. Online:https://n9.cl/i6xgz.